Sensorless multi-loop control of phase-controlled series-parallel resonant converter

Aboushady, A.A.; Ahmed, K.H.

Published in:
2014 International Conference on Renewable Energy Research and Application (ICRERA)

DOI:
10.1109/ICRERA.2014.7016435

Publication date:
2014

Document Version
Author accepted manuscript

Sensorless Multi-loop Control of Phase-Controlled Series-Parallel Resonant Converter

A.A.Aboushady
School of Engineering, University of Aberdeen, UK
On leave from Arab Academy for Science and Technology, Alexandria, Egypt
ahmed.aboushady@ieee.org

K.H.Ahmed
School of Engineering
University of Aberdeen
Aberdeen, United Kingdom
khaled@abdn.ac.uk

Abstract— **This paper proposes a multi-loop controller for the phase-controlled series-parallel resonant converter. Output voltage is solely measured for control and inner loop is used to enhance closed loop stability and dynamic performance compared to single-loop control. No additional sensors are used for inner loop variables. These are estimated using a Kalman filter, based on a linearized converter model. The advantage of this sensorless scheme is not only reducing the number of sensors but more significantly providing an alternative to sensing high frequency resonant tank variables which require high microcontroller resolution in real time. First, the converter non-linear large signal behavior is linearized using a state feedback based scheme. Consequently, the converter preserves its large signal characteristics while modeled as a linear system. Comparison is made between the most suitable state variables for feedback, according to a stability study. Finally, simulation and experimental results are demonstrated to validate the improved system performance in contrast with single-loop control.**

Keywords- **Large signal model, Phase control, Sensorless multi-loop control , Series-parallel resonant converter (SPRC).**

I. INTRODUCTION

Nowadays the demand for high power high voltage DC/DC converters for HVDC and DC grid applications has increased significantly, especially for grid integration of offshore wind parks [1]. Offshore wind has been growing rapidly in Europe in recent years and is likely to be one of the main future sources of energy, especially with increasing academic and governmental interest in European supergrid [2]. For the purpose of connecting offshore wind turbines to DC collection grids, transmitting power onshore, regulating power flow and providing galvanic isolation, DC/DC converters with unidirectional power capability are sufficient. Power density with footprint/weight issues is a key concern for offshore converters. For this reason, this article considers the series-parallel resonant converter (SPRC) as a candidate for offshore unidirectional DC/DC converters that satisfies high power density requirements due to its soft switching characteristics which enable high frequency operation.

The series-parallel resonant converter (SPRC) has been one of the main resonant converter topologies subject to rigorous research in the past [3-5]. It can operate over a large input voltage range and a large load range (no load to full load) while maintaining high efficiency. Several linear and non-linear control techniques have been reported for SPRC [6-9]; among them, the phase control technique [10-12] has been the most popular due to its constant frequency and simplicity in implementation with linear PI control.

In conventional single-loop PI control, high proportional gain is necessary to achieve high system robustness, disturbance rejection capability and dynamic performance. This results in lower closed loop stability margins and oscillatory system behaviour. To achieve better stability margins as well as improved dynamic characteristics, multi-loop control schemes have been used with power electronic converters [13,14]. By increasing the closed loop stability margin, loop gain can be increased to speed up system response and increase disturbance rejection capability [15]. In this paper, the single-loop output voltage PI controller in [16] is extended to include an inner control loop to enhance closed loop performance. However, using the high frequency resonant tank state variables of the SPRC for inner control loop realization is unpractical since much higher sampling (control) frequencies are required by the microcontroller in order to sample the variable used for control and convert it using PLL to an equivalent DC variable. This increases microcontroller computational burden and reduces the available code execution time. To solve this problem, the feedback state variable used for the inner control loop is not directly sensed but instead estimated using a Kalman filter based on a SPRC linearized large signal model. Full detail of this model is given in [16]. The proposed Kalman filter estimator eliminates the sensor required to measure the inner control loop feedback variable, hence achieving sensorless multi-loop SPRC control. Elimination of sensors has additional advantages including reduced cost, reduced possibility of single-point failure on sensor wiring and elimination of measurement errors [17]. This papers details the derivation of this sensorless Kalman filter-based controller while comparing which state variable is most suitable for inner control loop feedback according to a stability study. Simulation and experimental results are used to validate the proposed controller enhanced response in contrast with single-loop PI control.

II. SPRC LINEARIZED LARGE SIGNAL MODEL

Fig. 1 shows the circuit diagram for a typical SPRC. Two main subsystems exist; the AC sub-system (resonant tank and transformer) and the DC sub-system (output filter). In order to combine the AC and DC state variables into one model, it is essential to transform the AC state variables to equivalent DC quantities. This is achieved using the fundamental frequency approximation of the harmonic balance theory [18] which converts the AC state variables to *d-q* quantities. The resulting DC state variables from the resonant tank are combined with the natural DC state variables of the output filter side (modeled with conventional average state-space modeling) using a linearization scheme to overcome the non-linearity imposed by the rectifier. The result is an aggregate large signal linear model for the complete converter, which is given by (1) and detailed in [16].

$$\begin{aligned} \dot{\vec{x}}(t) &= A\vec{x}(t) + B\vec{u}(t) \\ y(t) &= C\vec{x}(t) \end{aligned} \tag{1}$$

where

$$\vec{x}(t) = [i_{Ld}\ i_{Lq}\ v_{Csd}\ v_{Csq}\ v_{Cpd}\ v_{Cpq}\ i_{Lo}\ v_o]^T,\ \vec{u}(t) = [v_c\ i_o]^T,\ y(t) = v_o,$$

$$A = \begin{bmatrix} -\frac{r_T}{L_T} & \omega_s & -\frac{1}{L_T} & 0 & -\frac{1}{L_T} & 0 & \frac{4k_3}{\pi L_T} & 0 \\ -\omega_s & -\frac{r_T}{L_T} & 0 & -\frac{1}{L_T} & 0 & -\frac{1}{L_T} & \frac{4k_7}{\pi L_T} & 0 \\ \frac{1}{C_s} & 0 & 0 & \omega_s & 0 & 0 & 0 & 0 \\ 0 & \frac{1}{C_s} & -\omega_s & 0 & 0 & 0 & 0 & 0 \\ \frac{1}{C_p} & 0 & 0 & 0 & 0 & \omega_s & -\frac{4}{\pi C_p} & 0 \\ 0 & \frac{1}{C_p} & 0 & 0 & -\omega_s & 0 & 0 & 0 \\ 0 & 0 & 0 & 0 & \frac{2}{\pi L_o} & 0 & -\frac{r_{Lo}}{L_o} & -\frac{1}{L_o} \\ 0 & 0 & 0 & 0 & 0 & 0 & \frac{1}{C_o} & 0 \end{bmatrix} \quad B = \begin{bmatrix} \frac{k_1}{L_T} & 0 \\ \frac{k_5}{L_T} & 0 \\ 0 & 0 \\ 0 & 0 \\ 0 & 0 \\ 0 & 0 \\ 0 & 0 \\ 0 & -\frac{1}{C_o} \end{bmatrix}$$

$$C = [0\ \ 0\ \ 0\ \ 0\ \ 0\ \ 0\ \ 0\ \ 1]$$

Using the derived model, control-to-output voltage transfer function can be approximated by the output filter circuit

$$\frac{v_o(s)}{v_c(s)} \approx \frac{2}{\pi}\frac{v_o(s)}{\bar{v}_{Br}(s)} \approx \frac{2}{\pi}\frac{1}{L_o C_o s^2 + r_{Lo} C_o s + 1} \tag{2}$$

This reduces the eighth order system model (1) to a second order model, thanks to the slow output filter dynamics which dominate converter output voltage response compared to the fast resonant tank dynamics. Discretizing the model (1) with a sampling time T_s, the discrete system can be represented by

$$\hat{x}(k+1) = A_d\hat{x}(k) + B_d u(k) \tag{3}$$

where

$$A_d = e^{AT_S},\ B_d = \int_0^{T_s} A(T_S - \tau)Bd\tau$$

$$\hat{x}(k) = [i_{Ld}\ i_{Lq}\ v_{Csd}\ v_{Csq}\ v_{Cpd}\ v_{Cpq}\ i_{Lo}\ v_o]^T$$

$$u(k) = [v_c\ i_o]^T$$

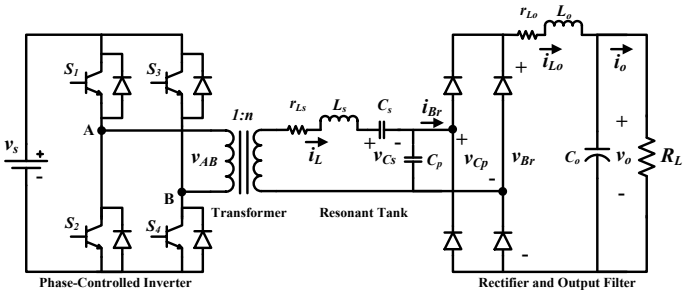

Fig. 1. Circuit diagram for the SPRC.

III. KALMAN FILTER BASED ESTIMATOR

This section details the implementation of the Kalman filter used to estimate the inner control loop state variable. The Kalman filter is a least-square estimator set to minimize the estimated error covariance [19,20]. Only the estimated state from the previous time step and the present measurement are needed to compute the estimate for the present state [21]. As such, the Kalman filter has two stages:

- *Predict* (time update): responsible for projecting forward in time the current state estimate for the next time step; and
- *Correct* (measurement update): responsible for using an actual noisy measurement to obtain a more accurate prediction of the next time step state estimate.

In the Kalman filter algorithm, the discrete system and measurement equations can be expressed by

$$x(k+1) = A_d x(k) + B_d u(k) + w(k) \tag{4}$$

$$z(k) = Hx(k) + v(k) \tag{5}$$

where $w(k)$ and $v(k)$ are the process and measurement noise matrices respectively. Their covariance matrices $Q(k)$ and $R(k)$ can be expressed by

$$Q(k) = E\left[w(k)w(k)^T\right],\ R(k) = E\left[v(k)v(k)^T\right] \tag{6}$$

H in the measurement equation (5) relates the state vector to the measurement $z(k)$. An estimate error $e(k)$ can be defined as

$$e(k) = x(k) - \hat{x}(k) \tag{7}$$

The estimate error covariance matrix is

$$P(k) = E\left[e(k)e(k)^T\right] \tag{8}$$

Fig. 2 shows the proposed control structure for the sensorless multi-loop output voltage controller of the SPRC. Fig. 3 depicts the algorithm for the Kalman filter based estimator. Steps for the calculation of the Kalman filter gain $L(k)$ are given in detail in [20].

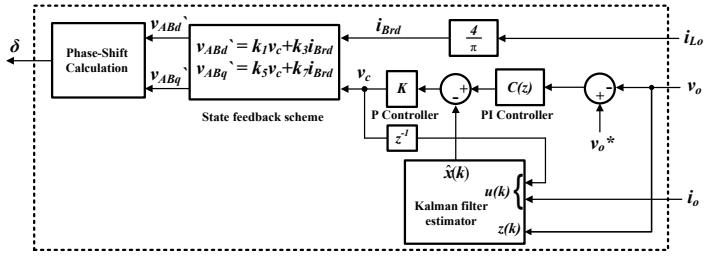

Fig.2. Proposed sensorless multi-loop output voltage controller of SPRC using Kalman filter based state estimator for inner loop.

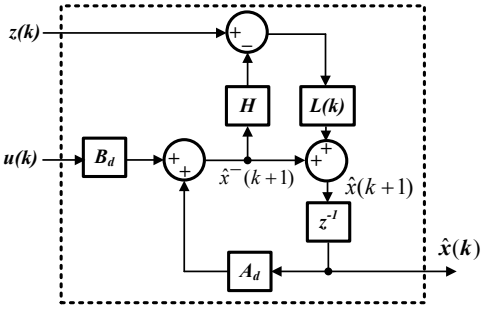

Fig.3 Kalman filter estimator.

The measurement $z(k)$ used for the correction update of the Kalman filter is the converter output voltage v_o as shown in Fig.2. The input vector $u(k)$ is comprised of the control v_c and load current i_o as denoted by (3).

IV. SELECTION OF INNER CONTROL LOOP STATE VARIABLE

The selection of the state variable x for the inner control loop is made according to a stability study of the closed loop system. The generic transfer function block diagram for the multi-loop control system is illustrated in Fig.4. The state variable x could be one of the following state variables: i_{Ld}, i_{Lq}, v_{Csd}, v_{Csq}, or v_{Cpd}.

A. D-axis inductor current feedback, i_{Ld}

Inner control loop feedback using i_{Ld} can be realized by taking $x(s)=i_{Ld}(s)$ in Fig.4. The transfer function $i_{Ld}(s)/v_o(s)$ can be obtained by solving (1) with i_o=0. Therefore, the closed loop transfer function can be expressed by

$$\frac{v_O(s)}{v_O^*(s)}=\frac{\frac{2}{\pi}KK_p\left(s+\frac{K_i}{K_p}\right)}{a_3s^4+a_2s^3+a_1s^2+\left(1+\frac{2}{\pi}KK_p\right)s+\frac{2}{\pi}KK_i} \tag{9}$$

$a_3=L_oC_oC_pK$, $a_2=r_{Lo}C_oC_pK+L_oC_o$, $a_1=KC_p+\frac{8C_oK}{\pi^2}+r_{Lo}C_o$.

B. Q-axis inductor current feedback, i_{Lq}

Taking $x(s)=i_{Lq}(s)$ and solving (1) with i_o=0, the closed loop transfer function is

$$\frac{v_O(s)}{v_O^*(s)}=\frac{\frac{2}{\pi}KK_p\left(s+\frac{K_i}{K_p}\right)}{a_2s^3+a_1s^2+\left(a_0+\frac{2}{\pi}KK_p\right)s+\frac{2}{\pi}KK_i} \tag{10}$$

$a_2=L_oC_o\left(1+K\omega C_p\right)$, $a_1=r_{Lo}C_o\left(1+K\omega C_p\right)$, $a_0=1+K\omega C_p$.

C. D-axis series capacitor voltage feedback, v_{Csd}

Taking $x(s)=v_{Csd}(s)$ and solving (1) with i_o=0, the closed loop transfer function can be expressed as

$$\frac{v_O(s)}{v_O^*(s)}=\frac{\frac{2}{\pi}KK_p\left(s+\frac{K_i}{K_p}\right)}{a_4s^5+a_3s^4+a_2s^3+a_1s^2+\left(a_0+\frac{2}{\pi}KK_p\right)s+\frac{2}{\pi}KK_i} \tag{11}$$

$a_4=-L_oC_oC_pL_TK$, $a_3=-r_{Lo}C_oC_pL_TK-L_oC_oC_pr_TK$,

$a_2=\frac{L_oC_oC_pK}{C_s}-r_{Lo}C_oC_pr_TK-L_TC_pK-\frac{8}{\pi^2}L_TC_oK+L_oC_o$,

$a_1=\frac{r_{Lo}C_oC_pK}{C_s}-r_TC_pK+r_{Lo}C_o$, $a_0=1+\frac{C_pK}{C_s}$

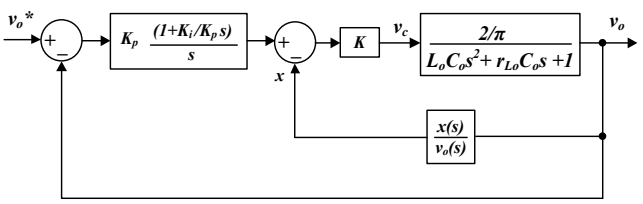

Fig.4 Generic transfer function block diagram for the multi-loop controller.

D. Q-axis series capacitor voltage feedback, v_{Csq}

Taking $x(s)=v_{Csq}(s)$ and solving (1) with i_o=0, the closed loop transfer function is

$$\frac{v_O(s)}{v_O^*(s)}=\frac{\frac{2}{\pi}KK_p\left(s+\frac{K_i}{K_p}\right)}{a_3s^4+a_2s^3+a_1s^2+\left(1+\frac{2}{\pi}KK_p\right)s+\frac{2}{\pi}KK_i} \tag{12}$$

$a_3=-L_oC_oC_p\omega L_TK$, $a_2=-r_{Lo}C_oC_p\omega L_TK+L_oC_o$,

$a_1=-2\omega L_TC_pK-\frac{8C_oK}{\pi^2\omega C_s}+r_{Lo}C_o$.

E. D-axis parallel capacitor voltage feedback, v_{Cpd}

Taking $x(s)=v_{Cpd}(s)$ and solving (1) with i_o=0, the closed loop transfer function is

$$\frac{v_O(s)}{v_O^*(s)}=\frac{\frac{2}{\pi}KK_p\left(s+\frac{K_i}{K_p}\right)}{a_2s^3+a_1s^2+\left(a_0+\frac{2}{\pi}KK_p\right)s+\frac{2}{\pi}KK_i} \tag{13}$$

$a_2=L_oC_o(1+K)$, $a_1=r_{Lo}C_o(1+K)$, $a_0=(1+K)$.

F. Stability study

The state variable used for inner control loop realization is selected by the closed loop system stability and closed loop bandwidth. Selection will be made from i_{Ld}, i_{Lq}, v_{Csd}, v_{Csq}, or v_{Cpd}. The root locus is used for the stability study. The characteristic equations of the closed loop transfer functions (9)-(13) are re-arranged to the form

$$1+K_pGH(s)=0 \tag{14}$$

$GH(s)$ is the open loop transfer function for which the root locus is plotted. Both continuous and discrete time domain root loci plots are illustrated in Fig.5 for all state variables.

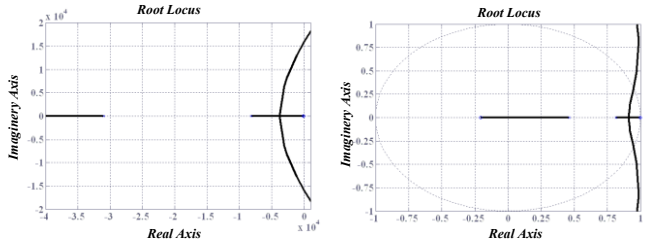

(a)

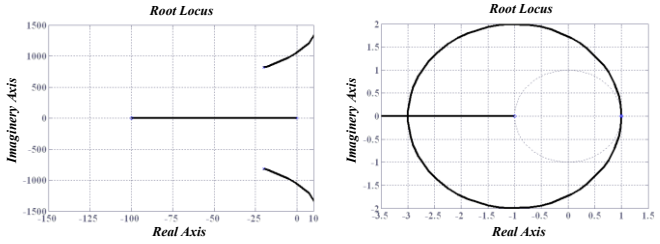

(b)

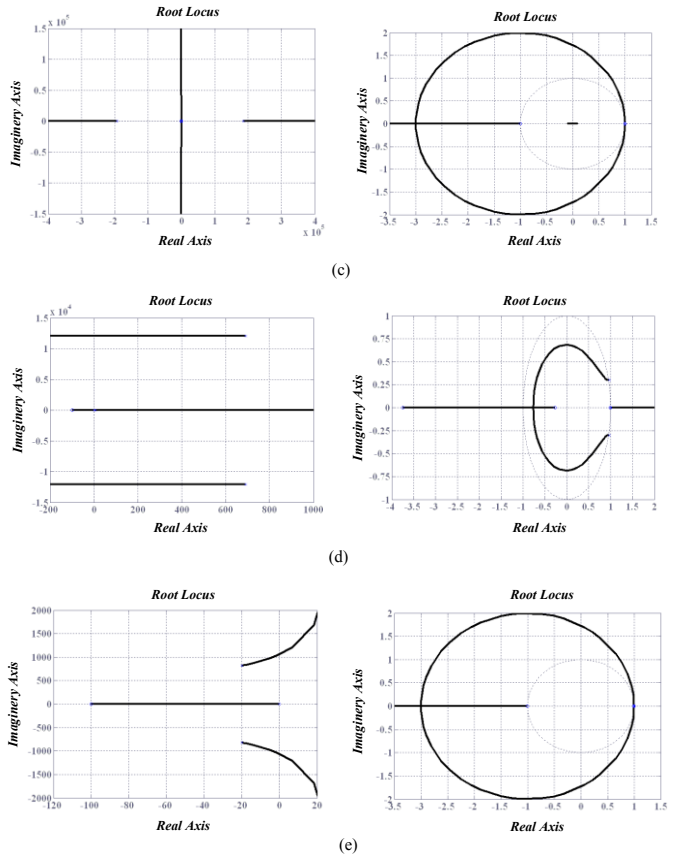

Fig.5 Root loci of multi-loop control system with the inner control loop state variable being (a) i_{Ld}, (b) i_{Lq}, (c) v_{Csd}, (d) v_{Csq}, and (e) v_{Cpd}.

The Kalman filter observer dynamics are much faster than the closed loop system; hence its effect is not included in the study. Fig.5 shows that using i_{Ld} for the inner control loop gives better closed loop margin of stability than the other state variables. Fig.6 shows a Bode plot of the closed loop bandwidth with the different state variables. Using i_{Ld} results in the highest closed loop bandwidth. Compared to single-loop PI control, bandwidth is increased with i_{Ld}. The higher bandwidth allows faster closed loop dynamic response and better disturbance rejection capability. Therefore, in terms of closed loop stability and bandwidth, it is confirmed that i_{Ld} is the best state variable for the inner control loop.

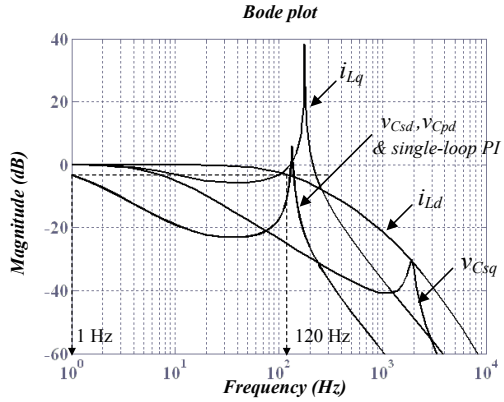

Fig.6 Bode plot illustrating closed loop bandwidth with the different state variables used for the inner control loop.

V. SIMULATION AND EXPERIMENTAL RESULTS

Fig. 7(a) shows the implementation of the proposed sensorless multi-loop SPRC output voltage controller both experimentally and in simulation. i_{Ld} is estimated using a Kalman filter observer and is the inner control loop feedback state variable. Table I summarizes the circuit and control parameter values. Measurements of the actual SPRC output voltage (v_o), output filter inductor current (i_{Lo}) and output (load) current (i_o) are taken.

Table I
SPRC parameters

Parameter	*Value*
Internal resistance of resonant tank inductor r_{Ls}	0.1916 Ω
Resonant tank inductance L_s	100.13 µH
Parasitic transformer resistance referred to secondary r_l	0.6 Ω
Transformer Leakage inductance referred to secondary L_l	9.12 µH
Total equivalent resistance $r_T=r_l+r_{LS}$	0.7916 Ω
Total equivalent inductance $L_T=L_l+L_s$	109.25 µH
Resonant tank series capacitance C_s	0.255 µF
Resonant tank parallel capacitance C_p	0.255 µF
Internal resistance of output filter inductor r_{Lo}	0.5 Ω
Output filter inductance L_o	12.5 mH
Output filter capacitance C_o	120 µF
Resonant tank fundamental frequency f_s	40 kHz
Sampling period T_s	25µs
Supply voltage v_s	60V
Transformer turns ratio n	0.5
Full-load power rating of experimental test rig	40W
Part-load resistive load R_{PL}	40.5 Ω
Full-load resistive load R_{FL}	14.4 Ω
Reference output voltage v_o^*	24V
Outer loop proportional gain K_p	0.1
Outer loop integral gain K_i	10
Inner loop proportional gain K	40

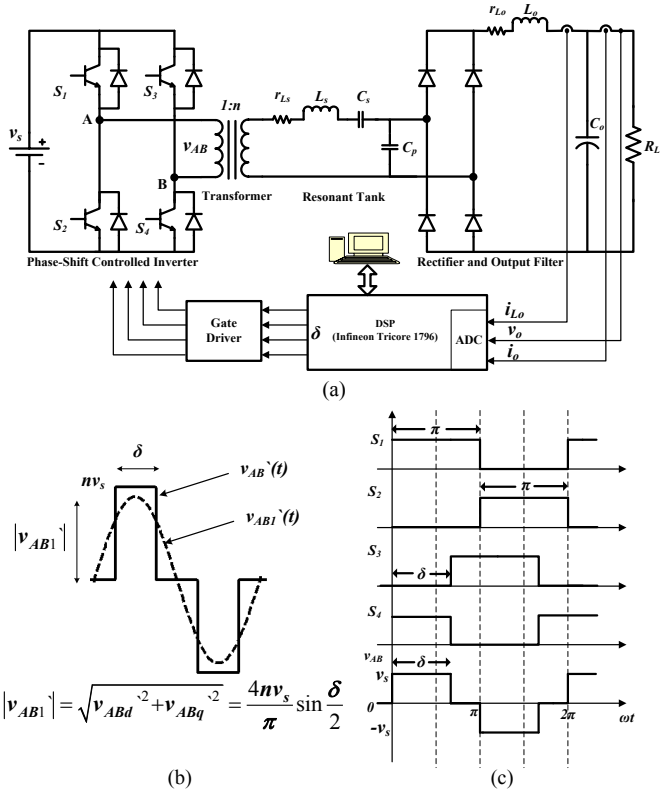

Fig. 7 Closed loop structure (a) circuit diagram, (b) phase-shift calculator, and (c) inverter phase control gating pattern.

Output voltage is measured to perform voltage control and correct Kalman filter state estimations ($z(k)$), output filter inductor current is measured for state feedback linearization as shown in Fig.2, and the load current is sensed for the Kalman filter input vector $u(k)$. The phase shift angle δ between the inverter legs (which is the output of the proposed controller in Fig.2) is calculated by the algorithm in Fig. 7(b). All inverter switches are switched with a fixed 50% duty cycle; the only control variable being the phase shift angle δ between S_1 and S_3 as shown in Fig. 7(c). This controls the effective inverter output voltage duty cycle.

For the sake of comparison with multi-loop controller performance, Fig. 8 shows simulation output voltage results for SPRC using single-loop PI controller [16] and Fig. 9 illustrates the output voltage using the multi-loop controller. Fig. 9(a) and (b) show at start-up, the output voltage reaches steady state in 40ms, compared to 1.0s for the single-loop PI control. At t=0.5s, a step load disturbance from partial load to full load is applied. Deviation from the reference output voltage (v_o^*=24V) is minimal compared to single-loop PI control where a high oscillatory response occurs at the step load instant. The high loop gain enhances the closed loop disturbance rejection, and steady state is restored after 100ms compared to 2.0s with single-loop PI control.

Fig.10 shows results for the remaining SPRC state variables implementing the sensorless multi-loop controller with i_{Ld} for inner control loop. These results can be compared with their counterpart obtained with single-loop PI control in [16]. Fig. 10(a) and (b) show output filter inductor current. Due to multi-loop control, dynamic response improved. At start-up, the current rises and reaches steady state in 25ms compared to 1.0s with the single-loop PI controller. The current increases after step load application and reaches steady state after 100ms compared to 2.0s with the single-loop PI case. The latter has a considerably higher oscillatory response. This verifies the increased closed loop stability margin introduced by the multi-loop controller. Fig.10 (c)-(h) show the resonant tank AC state variables i_L, v_{Cs} and v_{Cp}. Simulation and experimental results closely match. The Kalman filter observer gives accurate estimates of the state variables compared to the actual measurements. The proposed model is therefore useful for sensorless multi-loop control of the phase-controlled SPRC which is achieved without additional sensors compared to the single-loop PI controller.

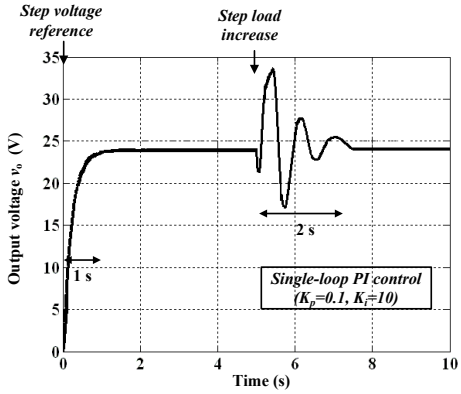

Fig. 8 Simulation result for SPRC output voltage using single-loop PI control.

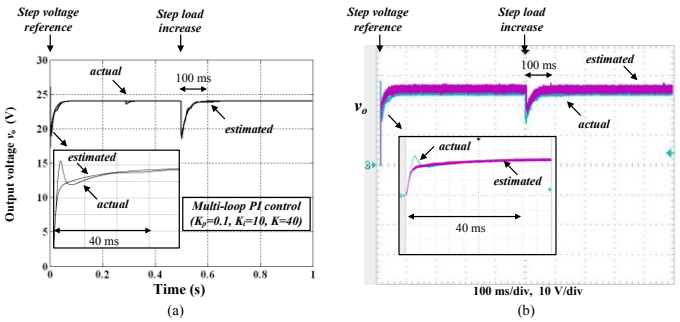

Fig. 9 Results for SPRC output voltage using the sensorless multi-loop PI control implementing i_{Ld} for inner control loop (a) Simulation, and (b) Experimental.

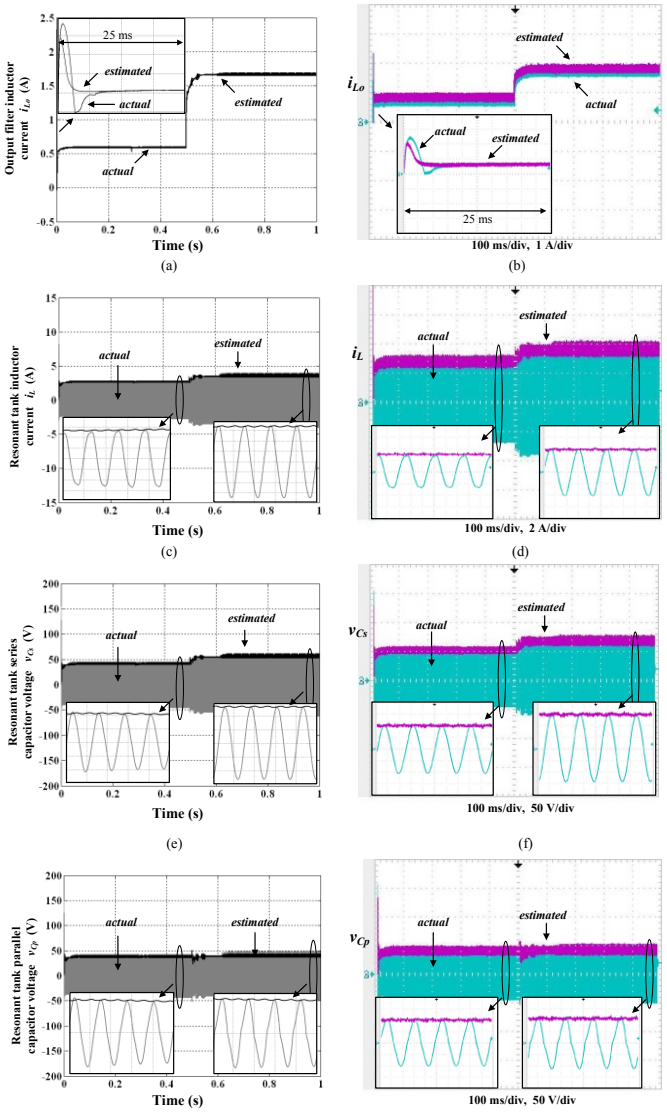

Fig. 10 Results for SPRC state variables (i_{Lo}, i_L, v_{Cs} and v_{Cp}) using the proposed sensorless multi-loop PI control implementing i_{Ld} for inner control loop (a),(c),(e)&(g) Simulation, and (b),(d),(f)&(h) Experimental.

VI. Conclusion

Single-loop PI control for SPRC output voltage regulation is simple to implement and gives acceptable closed loop

dynamics and steady state performance. However, the limitation on increasing the proportional gain is the stability of the resonant tank. This paper has proven that closed loop stability can be improved by using multi-loop control. To overcome the problems associated with sensing the high frequency resonant tank state variables (for inner control loop feedback) in real time microcontroller implementation, a sensorless scheme was proposed. This sensorless algorithm is based on a Kalman filter estimator derived from the linearized SPRC large signal model. The proposed sensorless multi-loop controller has shown enhancement of closed loop dynamics and stability margins with no additional sensors compared to single-loop control. Stability considerations and closed loop bandwidth have shown that i_{Ld} is the best state variable for inner control loop use. This was also verified with simulation and experimental results.

REFERENCES

[1] W. Chen, A.Q. Huang, C. Li, G. Wang, W. Gu, 'Analysis and Comparison of Medium Voltage High Power DC/DC Converters for Offshore Wind Energy Systems', IEEE Transactions on Power Electronics, Vol. 28, No. 4, pp. 2014 – 2023, 2013.

[2] Weixing Lu and BT Ooi, 'Optimal acquisition and aggregation of offshore wind power by multiterminal voltage-source HVDC', IEEE Transactions on Power Delivery, Vol. 18, No. 1, Jan 2003, pp 201 – 206.

[3] A. K. S. Bhat, "Analysis and design of a series-parallel resonant converter," Power Electronics, IEEE Transactions on, vol. 8, pp. 1-11, 1993.

[4] R. L. Steigerwald, "A comparison of half-bridge resonant converter topologies," Power Electronics, IEEE Transactions on, vol. 3, pp. 174-182, 1988.

[5] M. K. Kazimierczuk, N. Thirunarayan, and S. Wang, "Analysis of series-parallel resonant converter," Aerospace and Electronic Systems, IEEE Transactions on, vol. 29, pp. 88-99, 1993.

[6] C. L. Chia and E. K. K. Sng, "A Novel Robust Control Method for the Series-Parallel Resonant Converter," Power Electronics, IEEE Transactions on, vol. 24, pp. 1896-1904, 2009.

[7] C. Hao, E. K. K. Sng, and T. King-Jet, "Generalized Optimal Trajectory Control for Closed Loop Control of Series-Parallel Resonant Converter," Power Electronics, IEEE Transactions on, vol. 21, pp. 1347-1355, 2006.

[8] Z. Sanbao and D. Czarkowski, "Modeling and Digital Control of a Phase-Controlled Series-Parallel Resonant Converter," Industrial Electronics, IEEE Transactions on, vol. 54, pp. 707-715, 2007.

[9] J. L. Sosa, M. Castilla, J. Miret, L. Garcia de Vicuna, and J. Matas, "Modeling and Performance Analysis of the DC/DC Series-Parallel Resonant Converter Operating With Discrete Self-Sustained Phase-Shift Modulation Technique," Industrial Electronics, IEEE Transactions on, vol. 56, pp. 697-705, 2009.

[10] D. Czarkowski and M. K. Kazimierczuk, "Phase-controlled series-parallel resonant converter," Power Electronics, IEEE Transactions on, vol. 8, pp. 309-319, 1993.

[11] P. Jain, D. Bannard, and M. Cardella, "A phase-shift modulated double tuned resonant DC/DC converter: analysis and experimental results," in Applied Power Electronics Conference and Exposition, 1992. APEC '92. Conference Proceedings 1992., Seventh Annual, 1992, pp. 90-97.

[12] P. Jain, H. Soin, and M. Cardella, "Constant frequency resonant DC/DC converters with zero switching losses," Aerospace and Electronic Systems, IEEE Transactions on, vol. 30, pp. 534-544, 1994.

[13] R. B. Ridley, B. H. Cho, and F. C. Y. Lee, "Analysis and interpretation of loop gains of multiloop-controlled switching regulators [power supply circuits]," Power Electronics, IEEE Transactions on, vol. 3, pp. 489-498, 1988.

[14] R. D. Middlebrook, "Topics in Multiple-Loop Regulators and Current-Mode Programming," Power Electronics, IEEE Transactions on, vol. PE-2, pp. 109-124, 1987.

[15] M. G. Kim, D. S. Lee, and M. J. Youn, "A new state feedback control of resonant converters," Industrial Electronics, IEEE Transactions on, vol. 38, pp. 173-179, 1991.

[16] A. Aboushady, K. H. Ahmed, S. J. Finney, and B. W. Williams, "Linearized Large Signal Modeling, Analysis, and Control Design of Phase-Controlled Series-Parallel Resonant Converters Using State Feedback," Power Electronics, IEEE Transcations on, vol. 28, pp. 3896-3911, 2013.

[17] G. Ellis, Observers in Control Systems: Academic Press, September 2002.

[18] Z. M. Ye, P. K. Jain, and P. C. Sen, "Multiple frequency modeling of high frequency resonant inverter system," in Power Electronics Specialists Conference, 2004. PESC 04. 2004 IEEE 35th Annual, 2004, pp.4107-4113,Vol.6

[19] V. M. M. Saiz and J. B. Guadalupe, "Application of Kalman filtering for continuous real-time tracking of power system harmonics," Generation, Transmission and Distribution, IEE Proceedings-, vol. 144, pp. 13-20, 1997.

[20] G. Welch and G. Bishop. (2001). An Introduction to the Kalman Filter.

[21] K. K. C. Yu, N. R. Watson, and J. Arrillaga, "An adaptive Kalman filter for dynamic harmonic state estimation and harmonic injection tracking," Power Delivery, IEEE Transactions on, vol. 20, pp. 1577-1584, 2005.